# Growth and Post-Deposition Treatments of SrTiO$_3$ Films for Dye-Sensitized Photoelectrosynthesis Cell Applications

Robert W. Call,[†] Leila Alibabaei,[‡] Robert J. Dillon,[‡] Robin R. Knauf,[‡] Animesh Nayak,[‡] Jillian L. Dempsey,[‡] John M. Papanikolas,[‡] and Rene Lopez*,[†]

[†]Department of Physics and Astronomy, University of North Carolina at Chapel Hill, Chapel Hill, North Carolina 27599, United States

[‡]Department of Chemistry, University of North Carolina at Chapel Hill, Chapel Hill, North Carolina 27599, United States

ABSTRACT: Sensitized SrTiO$_3$ films were evaluated as potential photoanodes for dye-sensitized photoelectrosynthesis cells (DSPECs). The SrTiO$_3$ films were grown via pulsed laser deposition (PLD) on a transparent conducting oxide (fluorine-doped tin oxide, FTO) substrate, annealed, and then loaded with zinc(II) 5,10,15-tris(mesityl)-20-[(dihydroxyphosphoryl)phenyl] porphyrin (MPZnP). When paired with a platinum wire counter electrode and an Ag/AgCl reference electrode these sensitized films exhibited photocurrent densities on the order of 350 nA/cm^2 under 0 V applied bias conditions versus a normal hydrogen electrode (NHE) and 75 mW/cm^2 illumination at a wavelength of 445 nm. The conditions of the post-deposition annealing step—namely, a high-temperature reducing atmosphere—proved to be the most important growth parameters for increasing photocurrent in these electrodes.
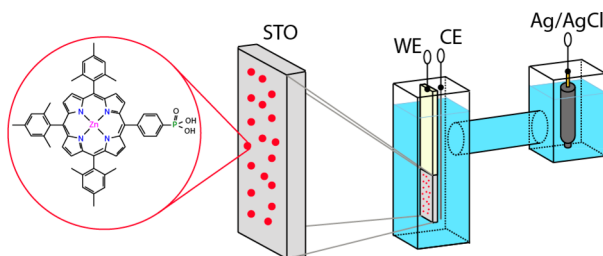
KEYWORDS: *SrTiO$_3$, pulsed laser deposition, post-deposition annealing, dye-sensitized photoelectrosynthesis cell, transient absorption*

I. INTRODUCTION

Photoelectrolysis of water via an irradiated semiconductor electrode was first observed in the late 1970s by using a TiO$_2$ electrode with an applied potential bias and ultraviolet illumination.[1,2] Shortly thereafter, single-crystal SrTiO$_3$ was identified as a possible photoelectrode for water splitting that required no applied bias.[3–5] Both TiO$_2$ and SrTiO$_3$ are wide-band-gap semiconductors making them more stable in a chemical environment than standard semiconductors but inefficient visible light collectors. Since these first reports of photoelectrolysis, there has been a widespread search for a semiconductor that can efficiently realize the same photo-chemistry under visible-light illumination without an applied bias. Dye-sensitized photoelectrosynthesis cells (DSPECs) provide a conceptual path to overcome the limitations of bare semiconductors.

In a DSPEC device, the photoelectrode is surface-loaded with light-absorbing dye that can pass photoexcited electrons to the electrode and a molecular catalyst that mediates the water oxidation reaction and is activated by the oxidized dye.[6–9] Proton reduction at a dark electrode completes the cell. For these devices, the semiconductor should have a wide bandgap and a conduction band edge energetically lower than the excited state of the dye. However, it should also have a conduction band potential that is more negative than the hydrogen reduction potential if water splitting is to be realized without an applied bias.[9] When studying only one of the two electrodes it is common practice to use a sacrificial reagent in the electrolyte to suppress back-electron transfer by quickly reducing the oxidized dye, thus avoiding the need to build up multiple oxidative equivalents.[10]

SrTiO$_3$ is a significantly less studied oxide semiconductor for dye-sensitized applications, compared to TiO$_2$. It is less favored because nanocrystalline TiO$_2$-based DSSCs have been proven to be extremely efficient at transporting electrons, giving rise to high photocurrent densities and high photoconversion efficiencies.[11,12] In addition, commonly used inorganic dyes that are functionalized with carboxylate or phosphonate anchors have a tendency to adsorb better onto TiO$_2$ than SrTiO$_3$.[9,12] Despite some of its inferior properties, SrTiO$_3$ has been noted to present a conduction band potential more capable of unbiased proton reduction. For this reason, doped and undoped SrTiO$_3$, grown by a variety of physical and chemical methods, has gained interest for use in direct excitation photoelectrochemical cells,[3,5,13–22] dye-sensitized solar cells,[11,12,23–31] and, in a more limited fashion, as an electrode for DSPECs.[32,33] The majority of studies utilizing SrTiO$_3$ in DSPECs have been limited to single-crystal electrodes. Single-crystal SrTiO$_3$ does not work well for DSPEC designs that require transparent electrodes. They are

also limited by low surface area for dye sensitization. Substantial work has been done on the effects of various post-deposition annealing conditions on single-crystal SrTiO₃ and SrTiO₃ films but few of these considered the effects on electrochemical behavior.[34−40] In particular, none examined the effects on dye-sensitized electrodes. Work on dye-sensitized SrTiO₃ films have not reported the effects of multiple post-deposition annealing conditions. This work provides a bridge between those investigations.

In this study, we have grown SrTiO₃ films utilizing pulsed laser deposition (PLD) and processed them under different annealing conditions to evaluate their properties as potential DSPEC photoanodes. Pulsed laser deposition can easily tailor film properties by varying material doping and controlling the sample's surface area.[41−52] The focus of this study is on attaining pure, compact SrTiO₃ films and varying the post-deposition factors. We have found that, despite an overall correct stoichiometric SrTiO₃ composition transfer from target to film by the PLD process, the resulting films (STO) are strontium rich on the surface. Post-deposition annealing conditions had strong effects on the measured flat-band potential of the STO films and the resulting photocurrent. When the films were annealed in hydrogen or air and loaded with a porphyrin dye, they yield a positive photocurrent under zero bias versus a normal hydrogen electrode (NHE) in a pH 6.1 solution. This was not the case for oxygen post-annealing, and the onset of the photocurrent is different for the different annealing atmospheres.

Films were studied using spectroscopic techniques, flat-band potential measurements, linear sweep voltammetry (LSV), and transient absorption. Correlation of results from these experiments grants insight into the dye-film interactions and the effects of changes in the film synthesis on those interactions. By comprehending these effects we can gain additional understanding about the prospects and limitations of SrTiO₃ films as photoanodes for DSPECs.

II. EXPERIMENTAL SECTION

STO films were grown in a PVD Products pulsed laser deposition system (NanoPLD) with a SrTiO₃ target (Kurt J. Lesker, 99.9% purity SrTiO₃, 5.06 g/cm³). The PLD process is carried out by focusing energetic laser pulses onto a target inside a chamber that can be evacuated or filled with a background gas. The absorbed laser light ablates material from the target surface, imparting a large amount of kinetic energy to ejected ions and atoms that then deposit onto a substrate held some distance away to grow a film. The PLD growth temperature was varied from 20 °C to 400 °C. All films were grown under 10 mTorr O₂ back-pressure on FTO substrates. After deposition, samples were annealed in air, hydrogen, or oxygen for 2 h. For pure gas annealing, the process was carried out in a MTI Corporation OTF-1200X tube furnace. The quartz tube was evacuated and then filled to above atmospheric pressure with either a 2.5% hydrogen, bulk argon mix or pure (99.99%) oxygen. Post-deposition temperature treatments in air were done using a MTI Corporation KSL-1200X box furnace. Annealing temperatures varied from 300 °C to 600 °C. For reference, previous work on single-crystal SrTiO₃ and chemically synthesized SrTiO₃ films often use annealing temperatures in excess of 600 °C to create oxygen vacancies and thus make samples n-type semiconductors.

STO films were sensitized with zinc(II) 5,10,15-tris(mesityl)-20[(dihydroxyphosphoryl) phenyl] porphyrin (MPZnP, see Figure 1) in order to improve visible-light induced photocurrent. Porphyrins have been shown to inject efficiently into other oxide materials used for photoanodes[53] and this particular dye was used because it is capable of injecting charge into high conduction band edges, making it
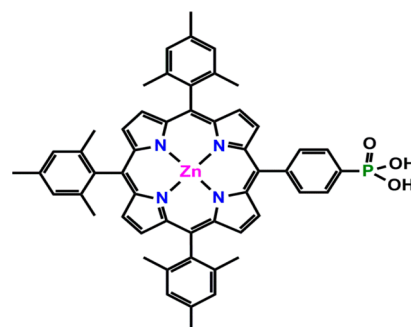
Figure 1. Composition of zinc(II) 5,10,15-tris(mesityl)-20-[(dihydroxyphosphoryl) phenyl] porphyrin used for visible-light absorption.

ideal for use with STO films.[54,55] Bare STO films were soaked in a 1:1 solution of 0.25 mM MPZnP dissolved in dichloromethane (DCM, Sigma−Aldrich) and 10 mM chenodeoxycholic acid dissolved in methanol (Sigma−Aldrich) for 22 h to sensitize films with the porphyrin. The chenodeoxycholic acid was employed to prevent excessive aggregation of dye molecules on the surface.[56] The amount of dye adsorbed to the surface was determined by UV absorption measurements with a Cary 50 Bio ultraviolet−visible (UV-vis) spectrophotometer. Using the Beer−Lambert law, we established the molar absorptivity of the dye when in solution (DCM). The amount of dye deposited on the film surface was estimated from those results by desorbing the sensitized dye from an electrode surface and measuring the absorbance.

Photocurrent measurements were performed with a potentiostat (CH Instruments, Model 760E), using a sensitized or unsensitized STO film as a working electrode, an Ag/AgCl reference electrode (Bioanalytical Systems, Inc., RE-5B, 3 M NaCl; 0.207 V vs NHE), and a braided Pt wire counter electrode. The working and counter electrodes were arranged inside a glass cuvette with a frit separating them from the compartment containing the reference electrode. Light for these experiments was provided by a Lumencor model Spectra light source (λ_{max} = 445 nm, 20 nm FWHM, variable power up to 75 mW; beam diameter = 0.8 cm). LSV and chronoamperometry were used to evaluate the photocurrents. LSVs were performed from −0.4 V to +0.4 V vs reference at 1 mV/s under 75 mW/cm² chopped light (445 nm) with 20 s intervals.

Flat-band potentials were measured with a Gamry Reference 600 potentiostat/galvanostat/ZRA in a 20 mL scintillation vial using the Mott−Schottky measurement technique described by Chen et al.[57] Both measurements were done at 22 ± 1 °C in an acetate buffer with 0.2 M LiClO₄. For photocurrent measurements, 20 mM ethylenedi-amine tetraacetic acid (EDTA) was included in the electrolyte to act as a reductive scavenger for the photoexcited semiconductor-dye complex to inhibit back-electron transfer and allow for the study of an isolated half-cell reaction.[6,7,58,59] For all photocurrent and flat-band potential experiments, the electrolyte was degassed for at least 30 min with argon. Photocurrents were measured in a pH 6.1 solution. Flat-band potential measurements were generally done in electrolyte of pH 5.8 with no EDTA added. To study flat-band potential change vs pH additional electrolytes of pH 2.4, 6.1, 9.3, 9.6, and 12.3 were used. The pH was controlled with NaOH or HCl as needed.

To obtain the flat-band potentials, a range of electrical potentials were applied to the photoelectrochemical cell with a small amplitude, sinusoidal perturbation at a set frequency while monitoring current to determine the impedance of the system. Several frequencies were used (100, 500, 1000 Hz) to ascertain that frequency dispersion had no significant effect on the results. A simple series RC circuit was assumed as the equivalent circuit to determine the capacitance of the space-charge layer from the impedance measurements. Using these results and the Mott−Schottky equation (eq 1), flat-band potentials can be obtained.

$$\frac{1}{C^2} = \frac{2}{\varepsilon_r \varepsilon_0 A^2 e N_D} \left(V - V_{fb} - \frac{k_B T}{e} \right) \tag{1}$$

where C is the capacitance at the working electrode, A the electrode area, N_D the donor density, V the applied potential, V_{fb} the flat-band potential, k_B the Boltzmann's constant, T the electrolyte temperature, and e the electric charge.

Ultrafast transient absorption experiments were performed with a femtosecond 1 kHz regeneratively amplified Ti:sapphire laser system (Clark, Model MXR 2210). The samples were excited with a 550 nm beam that was generated by diverting a portion of the 775 nm laser fundamental to a Topas-C optical parametric amplifier, followed by frequency doubling with a BBO crystal. Another portion of the beam was directed to a CaF_2 window to generate the white-light probe. Residual fundamental was removed from the probe with a low-pass filter. Experiments were performed with a magic-angle geometry of the pump and probe polarizations. The dye-loaded electrodes were placed in pH 5.8 acetate buffer in a sealed cuvette and sparged with Ar for 45 min. The cuvette was mechanically translated in the focal plane of the pump and probe beams for the duration of the experiment. Data were collected and analyzed using custom LabView software. Optical chirp was corrected by measuring the frequency resolved optical gating of a glass slide. The laser pump power at the sample was ≤ 0.6 mJ/cm^2.

Transient absorption experiments on the nanosecond time scale were performed as previously described.[60] Slides were immersed in pH 5.8 acetate buffer with 0.2 M $LiClO_4$ and then purged with argon for 40 min. Samples were excited at 555 nm, with a laser pulse energy of 4 mJ/pulse. Transient absorption spectra from 350 nm to 550 nm were generated from kinetic traces measured with a photomultiplier tube (PMT), because of the low sensitivity of the camera in this region. Kinetics were taken every 5−10 nm and were the result of averaging 40 laser shots.

X-ray photoelectron spectroscopy (XPS) (using a Kratos Axis Ultra DLD X-ray photoelectron spectrometer) was used to determine the STO composition on the film surface. The Sr:Ti ratio was determined by fitting high-resolution scans of the Sr 3d and Ti 2p peaks with a Shirley background and integrating. Calculated peak areas were combined with sensitivity factors from the Kratos Vision software to calculate atomic ratios. Film absorbance was measured using the same spectrophotometer used for dye-loading studies. X-ray diffraction (XRD) (Rigaku Multiflex, Source 1.5418 Å) provided insight into the crystallinity of films via 2θ measurements.

III. RESULTS AND DISCUSSION

A. Film Characterization. Films grown for this study were characterized with scanning electron microscopy (SEM), X-ray photoelectron spectroscopy (XPS), X-ray diffraction (XRD), and UV-vis absorption. SEM images provided film thickness measurements and confirmed that films were flat and dense (see Figure S1 in the Supporting Information). XPS data showed a Sr:Ti ratio of 1.5 on the surface of films annealed in 2.5% H_2 while XRD peaks indicate that the annealed films (all atmospheres) are indeed crystalline $SrTiO_3$ in the bulk (see Figures S2 and S3 in the Supporting Information). Post-deposition annealing and growth temperature caused noticeable changes in film crystallinity qualitatively assessed from the XRD scans. Samples annealed at 300 °C in hydrogen exhibited the $\langle 004 \rangle$ peak of anatase TiO_2. Phase separation in $SrTiO_3$ films grown by PLD has been observed previously but under dissimilar conditions.[34,61,62]

Strontium titanate stoichiometric crystals are expected to have a large band gap (~3.2 eV) and be transparent to visible light. Optical density measurements, corrected for reflection, scattering, and substrate contributions, show that the STO films grown for this study do absorb some light in the visible region (see Figure 2, as well as Figure S4 in the Supporting Information).
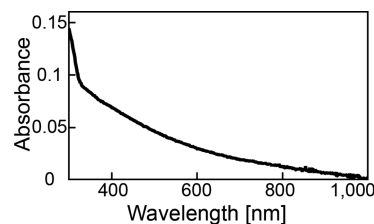

Figure 2. Absorption spectra for a thin (40 nm) STO film on quartz. The quartz substrate was used to discern the actual absorbance of STO below 400 nm (the glass substrate of FTO absorbs strongly in the UV). Sample was annealed at 500 °C in a 2.5% hydrogen atmosphere.

B. Flat-Band Potential Measurements. Flat-band potentials were determined from Mott−Schottky curves measured under the conditions described above (pH 5.8 electrolyte, Ag/AgCl reference electrode). The position of the flat-band potentials, relative to the water redox potential, can help evaluate the capacity of a semiconductor to split water under zero external bias, because they can be good approximations of the conduction band edge. For these films the post-deposition annealing step had the largest effect on the measured flat-band potential. In particular, annealing in a reducing environment led to more negative flat-band potentials (see Figures 3a and 3b), and higher temperatures led to larger carrier concentrations.

Samples were annealed in different environments to test the importance of annealing in a reducing atmosphere or oxidizing atmosphere. The hydrogen (reducing) environment yielded the most negative flat-band potentials, compared to samples annealed in oxygen or air. Film thickness and growth temperature had no noticeable effect on measured flat-band potentials. The change in flat-band potential vs pH of many metal oxides (including $SrTiO_3$) has been consistently reported as −59 mV/pH.[4,63,64] However, flat-band potential measurements of these STO films showed the same trend, contrary to previous work on $SrTiO_3$, the results for these films were consistently more positive than the hydrogen reduction potential at pH 5.8 (see Figure 3c).[4,65]

Because of the relatively high values of the measured flat-band potentials, the approximate conduction band edges from these results are calculated to be more positive than the hydrogen reduction potential. This does not necessarily mean that these films will require large applied biases to function as DSPEC electrodes, because flat-band potential measurements can be an imprecise tool for this approximation. A more complex equivalent circuit might be required to interpret the impedance data or ions adsorbed on the film surface are known to shift measured flat-band potentials.[66] Previous work, measuring flat-band potentials for TiO_2, illustrates how reported flat-band potentials can vary by hundreds of millivolts for nominally the same material.[4,55] Thus, while the absolute values depart from our expectations, the change in flat-band potential vs pH follows the well-established trend. This lends confidence to the relative positions of the flat-band potentials, namely, that samples annealed in hydrogen have higher conduction band edges than those annealed in air or oxygen.

Carrier concentration calculations can also be made from the Mott−Schottky equation. Applying this analysis reveals a dramatic increase in carriers following the annealing process. These measurements reflect an increase in doping for annealed films. Annealed films had carrier concentrations on the order of 10^{19} per cm^2. This is similar to previous reports of carrier
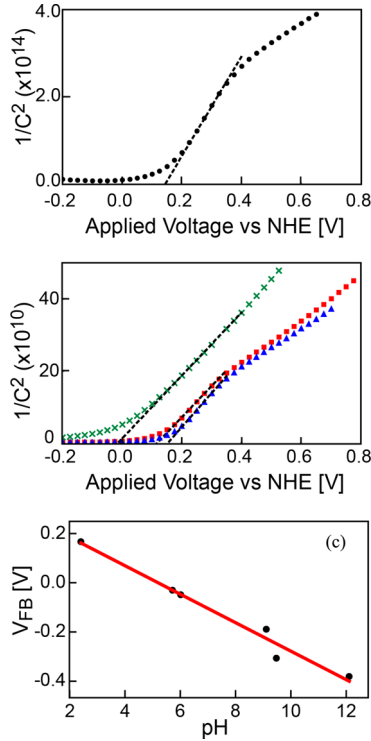
Figure 3. (a, b) Data from flat-band potential measurements done at 1 kHz (pH 5.8 electrolyte) for 1.7-μm-thick STO films that were not annealed (denoted as solid circles, ●) or annealed at 500 °C in oxygen (denoted by solid squares, ■), hydrogen (denoted by cross symbols, ✕), or air (denoted by solid triangles, ▲). Dashed black lines indicate linear fits that are used for calculating flat-band potentials ($V_{fb,●}$ = 117 ± 2 mV, $V_{fb,▲}$ = 96 ± 2 mV, $V_{fb,✕}$ = −45 ± 7 mV, $V_{fb,■}$ = 122 ± 3 mV) and carrier concentrations ($\eta_{●}$ = (410 ± 8) × 10^{14} electrons/cm^2, $\eta_{▲}$ = (510 ± 8) × 10^{17} electrons/cm^2, η_{x} = (55 ± 2) × 10^{18} electrons/cm^2, $\eta_{■}$ = (51 ± 2) × 10^{18} electrons/cm^2). (See Table S1 in the Supporting Information for additional measurements.) (c) Flat-band potential vs pH for STO films annealed in hydrogen. Fit: (V_{fb}) = 302 mV − (59 mV/pH) × pH.

concentration for annealed single-crystal SrTiO$_3$.[4,32,67] Samples annealed in different atmospheres had carrier concentrations that were statistically the same when averaged across multiple frequencies. This is unusual, because of the different doping processes that occur in the different atmospheres (i.e., reduction in the hydrogen atmosphere and oxidation in the air or oxygen atmospheres). This result, coupled with the trend in flat-band potential, suggests that reduction and oxidation can result in similar increases in dopant concentration but the energies of the dopant states are significantly different. Previous studies on the effects of annealing atmosphere on SrTiO$_3$ have shown that annealing in hydrogen will lead to oxygen vacancies in the lattice structure,[37,39,67,68] while annealing in air or oxygen leads to a variety of oxygen defects.[34,69−72]

C. Photocurrent Measurements. Direct photocurrent measurements were employed to determine the required applied potential to achieve positive anodic photocurrent from the sensitized films under visible-light illumination. A film that requires a small, or 0 V, applied voltage will have a better chance of success in a bias-free DSPEC cell than a film that requires an applied bias of hundreds of millivolts. MPZnP was chosen as the sensitizer because, as stated above, its photoexcited state should be capable of injecting an electron into the high conduction band of SrTiO$_3$. It also has a

phosphonic acid functional group that provides an anchoring site for binding to the STO surface and a high molar absorption coefficient.[54,55] Photocurrent measurements were performed in the presence of EDTA, which acts as a reductive scavenger, regenerating the porphyrin chromophore after excitation and injection have occurred. This reduces charge recombination between the injected electron and oxidized dye, allowing the charge carriers to diffuse to the FTO back contact.

Dye was loaded onto the films via submersion in a solution containing MPZnP and chenodeoxycholic acid. UV-vis absorption was used to monitor samples during dye loading and determine the adsorption isotherm of the dye. Absorbance for all samples plateaued within 22 h of being submerged. Several dye-loaded samples were desorbed in dichloromethane and the absorption of the desorbing solution was compared to solutions with known dye concentrations to determine the number of molecules on the surface (3.44 ± 0.22 × 10^{14} molecules/cm^2). The loading is a factor of 100 less than that found for similar porphyrin chromophores on mesoporous metal-oxide films[60] and is a factor in the magnitude of photocurrents measured below. Utilizing estimates for the size and packing density of the molecules reveals that there is too much dye to only form one monolayer, indicating that the chenodeoxycholic acid permitted some aggregation of the MPZnP. Absorption measurements of loaded films grown with different thicknesses and post-deposition annealing conditions were very similar, indicating that there were similar densities of molecules attached to all of the films (see Figure S5 in the Supporting Information). Dye-loaded STO was also compared to MPZnP-loaded films of TiO$_2$ grown under the same pulsed laser deposition conditions. The TiO$_2$ did load better, which is a result that is expected based on the work by Burnside et al. (see Figure S6 in the Supporting Information).[12]

To confirm that the photocurrent observed for the dye-loaded films stemmed from sensitization, photocurrents were measured for bare STO films and for FTO substrates. Bare STO films, as shown in Figure 2, absorb some light at 445 nm and were found to produce photocurrent on the order of nA/cm^2. The series of experiments to determine the photocurrent contribution of MPZnP and the STO film itself is summarized in Table 1. The dye-sensitized STO electrodes exhibit substantially higher photocurrents, compared to the bare STO films. Annealing the STO film electrodes in hydrogen

Table 1. Visible-Light Photocurrent Measurements of Films Annealed in 2.5% Hydrogen

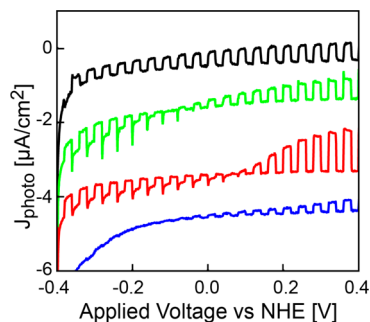| substrate	anneal temp (°C)	dye	photocurrent (nA/cm^2)[a]		
			15 mW/cm^2	50 mW/cm^2	75 mW/cm^2
FTO	500		3.0	7.0	7.0
FTO	500	MPZnP	−13	0.2	13
STO			2.0	5.0	5.0
STO	500		22	55	80
STO	300	MPZnP	20	40	50
STO	500	MPZnP	50	170	250
STO	600	MPZnP	50	230	360

[a]0.2 V vs NHE applied voltage; 445 nm illumination at three different intensities. Measurements were taken by subtracting the dark current from photocurrents 10 s after initial illumination in order to allow the system to come to equilibrium. See Figure S7 in the Supporting Information for plots of the associated photocurrent curves.

causes the most substantial increase in photocurrent (by a factor of 10). These results simultaneously confirm that the annealing step is very important for improving the photocurrent for these STO films and that sensitization with MPZnP yields a significant contribution to the photocurrent. Annealed, sensitized films illuminated with a 1.5 AM solar simulator (0.1 sun intensity at the electrode with a 400 nm wavelength cutoff filter to exclude direct UV excitation) had photocurrent densities on the order of 5 nA/cm^2 and exhibited significantly more noise than those illuminated with the intense blue light source. No more measurements with the solar simulator were pursued.

The effects of annealing temperature were studied by measuring photocurrent from films that had been annealed in 2.5% hydrogen at three different temperatures (300, 500, and 600 °C) and were then sensitized with MPZnP. This revealed a trend of increasing photocurrent for higher annealing temperatures, which correlates well with the increase in measured carrier concentration for films annealed at higher temperatures. However, for samples annealed in 2.5% hydrogen at 600 °C, the resistance of the FTO substrate increased by 1000-fold. If this change in the resistivity of the conductive substrate could be avoided, the increase in photocurrent for higher annealing temperatures would probably be greater.

Film thickness and growth temperature were also studied to observe their effect on photocurrent (Figures S8 and S9 in the Supporting Information). Thickness is important because it determines the distance that electrons must travel through the resistive film to reach the transparent conducting oxide. Photocurrent measurements for films varying from 400 nm to 3.5 μm showed that, even for the thickest films, the reduction in photocurrent was not large (by no more than a factor of ~2). High growth temperatures usually allow atoms to move more freely on the film surface after deposition, producing more compact films. However, in these experiments, the effects of increasing the growth temperature did not yield a clear trend.

Using these studies as a guide, several films were produced with optimal properties for maximizing photocurrent. By performing LSV on these samples under periodic illumination, we can determine the range of voltages required for obtaining positive photocurrents. Figure 4 shows linear sweep voltammograms from −0.4 V to 0.4 V (vs NHE). Hydrogen-annealed samples maintain a positive photocurrent, while samples
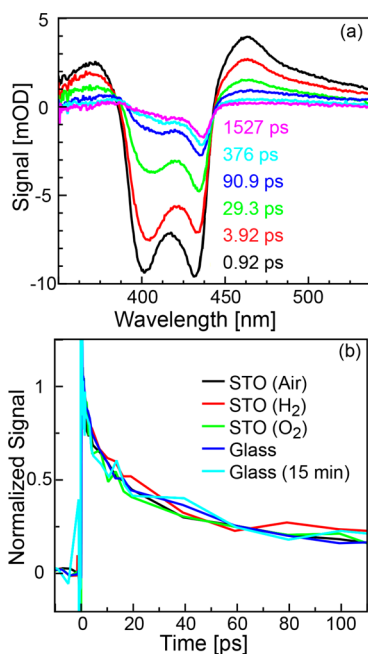
annealed in air and oxygen do not start yielding a positive photocurrent until −70 ± 5 mV and 90 ± 5 mV, respectively. This does not definitively mean that a DSPEC device using the hydrogen films could run with no external bias as other losses would appear in a complete water splitting operation and the photocurrents for these films are far too small. However, this result is a positive indication that the application might be possible if the photocurrent could be increased substantially. The highest photocurrent density in this experiment for an applied potential of 0 V vs NHE came from the sensitized sample annealed in hydrogen. It yielded 350 nA/cm^2 above the dark level for 75 mW/cm^2 illumination at a wavelength of 445 nm.

As seen in Figure 4, depending on the annealing conditions and applied potential, the sensitized electrodes exhibited photoanodic or photocathodic behavior, indicative of either an electron or hole injection process, respectively. This dual behavior has been observed previously in nonsensitized systems.[73−75] These results correlate well with the Mott−Schottky analysis, which showed that the conduction band edges of these samples changed, depending on the post-deposition annealing atmosphere with hydrogen and air-annealed samples having more negative conduction band edges than oxygen-annealed samples. Evidently less applied potential is required for electron injection into the samples with more negative conduction band edges.

D. Transient Absorption Spectroscopy. Transient absorption (TA) experiments were employed to further investigate the photoresponse of these sensitized STO films. TA is commonly used to investigate the charge injection of dye into the semiconductor substrate. Given the low measured photocurrent densities (disproportionally low, even after considering the limited surface area), this raises the concern of whether or not MPZnP is efficiently injecting charge into the STO film. In previous work, it has been shown that injection from singlet states of porphyrin chromophores is in competition with loss to triplet states in the dye.[60]

TA experiments were conducted in pH 5.8 acetate buffer with 0.2 M LiClO$_4$ in order to assess the injection dynamics and match with the photocurrent measurements. A dye-loaded nonconductive glass slide was selected as the most appropriate control sample. Figure 5 shows a representative plot of the time-resolved signal for the STO samples, along with normalized kinetics for each sample. The observed photophysics for the STO samples were the same, regardless of annealing treatment, and furthermore, were the same as a dye-loaded inert glass sample. The rapid decays, compared to nanosecond solution lifetimes, and other observations suggest that chromophore−chromophore interactions dominate the observable photophysics, obscuring any electron or hole injection.[76,77] The overall shape of the earliest transient spectrum contains two negative peaks at 405 and 432 nm and does not resemble the ground-state absorption spectrum, which has only one peak at 428 nm. The negative peaks evolve over time, converging to a long-lived single negative peak at 436 nm. The induced absorption peaks at 380 nm and 450−650 nm relax with the same overall time constant as the bleach (see Figure S10 in the Supporting Information), but do not significantly change in shape. The kinetics are multiexponential containing a fast component with an average lifetime of 30 ps and a small portion (~8%) of long-lived multiexponential signal due to injection that persists with $\langle t \rangle = 15-30$ μs, depending on the annealing atmosphere (see Figure S11 in the Supporting

Figure 4. Offset linear sweep voltammograms from −400 mV to 400 mV (vs NHE) of dye-sensitized STO films (1.7 μm thick, grown with 10 mTorr oxygen back-pressure) annealed to 500 °C in different atmospheres [from top to bottom: hydrogen, air, oxygen, hydrogen (unsensitized)] periodically illuminated with 445 nm light (75 mW/cm^2). Measurements were done in pH 6.1 solution of 0.2 M LiClO$_4$ and 20 mM EDTA with an acetate buffer.

Figure 5. (a) Evolution of the transient signal for the O_2-annealed STO sample from 0.92 ps to 1527 ps after illumination (this time evolution was similar, regardless of the annealing film conditions). (b) Normalized kinetics traces for the 460 nm induced absorption for various sensitized STO films and the sensitized inert glass.

Information). The spectra and lifetimes are comparable to previously reported results for Zn porphyrins anchored to TiO_2.[77−79]

In an attempt to limit the extent of chromophore aggregation, a second set of samples was prepared with reduced dye-loading times (from 22 h to 15 min). For these samples, the early time bleach is not split and more closely resembles the ground-state absorption (Figure S12 in the Supporting Information); however, the excited-state spectrum still changes over time and the decay kinetics remain the same as the original samples, indicating that the observed signal still originates primarily from chromophore−chromophore inter-action. Samples showed reductions in photocurrent as they were loaded for longer amounts of time, despite having increased amounts of dye (Figure S13 in the Supporting Information). Lower photocurrent for longer dye-loading time has been observed previously for Zn porphyrins on TiO_2.[78] Our results suggest only a small minority of monomer chromo-phores interact with the STO, and longer loading time depletes these monomers lowering the photocurrent. The ultrafast dynamics was found to be almost identical in the sensitized STO films and a sensitized inert glass sample. This indicates, contrary to expectations, that the charge injection from the MPZnP chromophore into the STO films is highly inefficient. The aggregation of MPZnP on these samples seems to be a very significant problem, prompting the decreased photo-currents, despite the presence of chenodeoxycholic acid.

IV. CONCLUSIONS

This study investigated the applicability of pulsed laser deposition (PLD)-grown STO films on FTO substrates as photoanodes for DSPEC devices, with particular emphasis on the effects of annealing temperature and atmosphere on film performance. We observed an increase in photocurrent with higher-temperature post-deposition anneals and differences in electrode performance that are due to the annealing atmosphere. Post-deposition annealing in air or oxygen led to films with more positive flat-band potentials that could exhibit photocathodic or photoanodic behavior, depending on the applied bias. Bolts and Wrighton found that measured flat-band potentials for single-crystal metal oxides corresponded closely with the onset of photoanodic currents; however, in this work on $SrTiO_3$ films, that conclusion is not supported.[4] This work illustrates the importance of the post-deposition anneal, with a clear shift toward more negative flat-band potentials in reducing annealing conditions and overall better photocurrents with increasing processing temperatures.

Photocurrent measurements of sensitized films showed an increase in photocurrent, compared to nonsensitized films, indicating that charge injection from the MPZnP does occur. However, ultrafast and nanosecond scale transient absorption measurements showed that the MPZnP sensitizer did not efficiently inject charge into the STO films, probably because of dye aggregation and chromophore−chromophore interactions. The maximum achieved photocurrent with 0 V applied bias (vs NHE) was 350 nA/cm^2 under 75 mW/cm^2 illumination (445 nm). This result, combined with absorption measurements of sensitized films (Figure S5), leads to a calculated internal quantum efficiency of <0.01%.

Based on observations made during this study, there are several paths that can be taken to improve the performance of these electrodes. Effects of even-higher annealing temperatures should be examined, but that will require a different substrate capable of maintaining low resistivity during a high-temperature anneal in a hydrogen atmosphere. The surface area of these films can be increased, allowing for more sensitization, by altering the back-pressure during the pulsed laser deposition process or by other large-areal-density thin-film fabrication routes. Beyond the film itself, identifying a more suitable dye for improved charge injection and reduced dye aggregation would be required to significantly improve these electrodes and make them more competitive as perspective dye-sensitized photoelectrosynthesis cells (DSPECs) photoanodes.

■ ASSOCIATED CONTENT

Ⓢ Supporting Information

The Supporting Information is available free of charge on the ACS Publications website at DOI: 10.1021/acsami.6b01289.

> SEM image of STO film; XRD and XPS spectra of bare STO films; UV-vis spectra of MPZnP-loaded STO films of different thickness and a TiO_2 film grown by PLD; photocurrent measurements of STO films of different thickness and grown at different temperatures; transient absorption data of MPZnP-loaded STO films and MPZnP-loaded glass; photocurrent measurements of a STO film loaded with progressively larger amounts of MPZnP (PDF)

■ AUTHOR INFORMATION

Corresponding Author
*E-mail: rln@physics.unc.edu.

Notes
The authors declare no competing financial interest.

■ REFERENCES

(1) Fujishima, A.; Honda, K. Electrochemical Photolysis of Water at a Semiconductor Electrode. *Nature* **1972**, *238*, 37−38.

(2) Nozik, A. J. Photoelectrolysis of Water Using Semiconducting TiO_2 Crystals. *Nature* **1975**, *257*, 383−386.

(3) Wrighton, M. S.; Ellis, A. B.; Wolczanski, P. T.; Morse, D. L.; Abrahamson, H. B.; Ginley, D. S. Strontium Titanate Photoelectrodes. Efficient Photoassisted Electrolysis of Water at Zero Applied Potential. *J. Am. Chem. Soc.* **1976**, *98*, 2774−2779.

(4) Bolts, J. M.; Wrighton, M. S. Correlation of Photocurrent-voltage Curves with Flat-band Potential For Stable Photoelectrodes for the Photoelectrolysis of Water. *J. Phys. Chem.* **1976**, *80*, 2641−2645.

(5) Mavroides, J. G.; Kafalas, J. a.; Kolesar, D. F. Photoelectrolysis of Water in Cells with $SrTiO_3$. Anodes. *Appl. Phys. Lett.* **1976**, *28*, 241−243.

(6) Youngblood, J. W.; Lee, S. H. A.; Kobayashi, Y.; Hernandez-Pagan, E. a.; Hoertz, P. G.; Moore, T. a.; Moore, A. L.; Gust, D.; Mallouk, T. E. Photoassisted Overall Water Splitting in a Visible Light-Absorbing Dye-Sensitized Photoelectrochemical Cell. *J. Am. Chem. Soc.* **2009**, *131*, 926−927.

(7) Youngblood, W. J.; Lee, S.-H. A.; Maeda, K.; Mallouk, T. E. Visible Light Water Splitting Using Dye-sensitized Oxide Semiconductors. *Acc. Chem. Res.* **2009**, *42*, 1966−1973.

(8) Alibabaei, L.; Brennaman, M. K.; Norris, M. R.; Kalanyan, B.; Song, W.; Losego, M. D.; Concepcion, J. J.; Binstead, R. A.; Parsons, G. N.; Meyer, T. J. Solar Water Splitting in a Molecular Photoelectrochemical Cell. *Proc. Natl. Acad. Sci. U. S. A.* **2013**, *110*, 20008−20013.

(9) Alibabaei, L.; Luo, H.; House, R. L.; Hoertz, P. G.; Lopez, R.; Meyer, T. J. Applications of Metal Oxide Materials in Dye Sensitized Photoelectrosynthesis Cells For Making Solar Fuels: Let the Molecules Do the Work. *J. Mater. Chem. A* **2013**, *1*, 4133−4145.

(10) Song, W.; Ito, A.; Binstead, R. a.; Hanson, K.; Luo, H.; Brennaman, M. K.; Concepcion, J. J.; Meyer, T. J. Accumulation of Multiple Oxidative Equivalents at a Single Site by Cross-surface Electron Transfer on TiO_2. *J. Am. Chem. Soc.* **2013**, *135*, 11587−11594.

(11) Bandara, J.; Weerasinghe, H. Enhancement of Photovoltage of Dye-sensitized Solid-State Solar Cells by Introducing High-Band-Gap Oxide Layers. *Sol. Energy Mater. Sol. Cells* **2005**, *88*, 341−350.

(12) Burnside, S.; Moser, J.; Brooks, K.; Gratzel, M.; Cahen, D. Nanocrystalline Mesoporous Strontium Titanate as Photoelectrode Material for Photosensitized Solar Devices: Increasing Photovoltage Through Flatband Potential Engineering. *J. Phys. Chem. B* **1999**, *103*, 9328−9332.

(13) Hara, S.; Yoshimizu, M.; Tanigawa, S.; Ni, L.; Ohtani, B.; Irie, H. Hydrogen And Oxygen Evolution Photocatalysts Synthesized from Strontium Titanate by Controlled Doping and Their Performance in Two-Step Overall Water Splitting Under Visible Light. *J. Phys. Chem. C* **2012**, *116*, 17458−17463.

(14) Hara, S.; Irie, H. Band Structure Controls of $SrTiO_3$ Towards Two-Step Overall Water Splitting. *Appl. Catal., B* **2012**, *115−116*, 330−335.

(15) Zhao, L.; Fang, L.; Dong, W.; Zheng, F.; Shen, M.; Wu, T. Effect of Charge Compensation on the Photoelectrochemical Properties of Ho-Doped $SrTiO_3$ Films. *Appl. Phys. Lett.* **2013**, *102*, 121905.

(16) Kawasaki, S.; Nakatsuji, K.; Yoshinobu, J.; Komori, F.; Takahashi, R.; Lippmaa, M.; Mase, K.; Kudo, A. Epitaxial Rh-Doped $SrTiO_3$ Thin Film Photocathode for Water Splitting under Visible Light Irradiation. *Appl. Phys. Lett.* **2012**, *101*, 033910.

(17) Townsend, T. K.; Browning, N. D.; Osterloh, F. E. Nanoscale Strontium Titanate Photocatalysts for Overall Water Splitting. *ACS Nano* **2012**, *6*, 7420−7426.

(18) Shi, J.; Ye, J.; Ma, L.; Ouyang, S.; Jing, D.; Guo, L. Site-selected Doping of Upconversion Luminescent Er^{3+} into $SrTiO_3$ for Visible-Light-Driven Photocatalytic H_2 or O_2 Evolution. *Chem.—Eur. J.* **2012**, *18*, 7543−7551.

(19) Arai, T.; Sato, S.; Kajino, T.; Morikawa, T. Solar CO_2 Reduction Using H_2O by a Semiconductor/Metal-Complex Hybrid Photocatalyst: Enhanced Efficiency and Demonstration of a Wireless System Using $SrTiO_3$. Photoanodes. *Energy Environ. Sci.* **2013**, *6*, 1274−1282.

(20) Pinheiro, A. N.; Firmiano, E. G. S.; Rabelo, A. C.; Dalmaschio, C. J.; Leite, E. R. Revisiting $SrTiO_3$ as a Photoanode for Water Splitting: Development of Thin Films with Enhanced Charge Separation under Standard Solar Irradiation. *RSC Adv.* **2014**, *4*, 2029−2036.

(21) Kawasaki, S.; Takahashi, R.; Akagi, K.; Yoshinobu, J.; Komori, F.; Horiba, K.; Kumigashira, H.; Iwashina, K.; Kudo, A.; Lippmaa, M. Electronic Structure and Photoelectrochemical Properties of an Ir-Doped $SrTiO_3$ Photocatalyst. *J. Phys. Chem. C* **2014**, *118*, 20222−20228.

(22) Yin, J.; Ye, J.; Zou, Z. Enhanced Photoelectrolysis of Water with Photoanode $Nb:SrTiO_3$. *Appl. Phys. Lett.* **2004**, *85*, 689−691.

(23) Kim, C. W.; Suh, S. P.; Choi, M. J.; Kang, Y. S.; Kang, Y. S. Fabrication of $SrTiO_3$−TiO_2 Heterojunction Photoanode with Enlarged Pore Diameter for Dye-Sensitized Solar Cells. *J. Mater. Chem. A* **2013**, *1*, 11820−11827.

(24) Li, Y. Y.; Hao, H. S.; Qin, L.; Wang, H. L.; Nie, M. Q.; Hu, Z. Q.; Gao, W. Y.; Liu, G. S. Synthesis and Characterization of Ho^{3+}-Doped Strontium Titanate Downconversion Nanocrystals and Its Application in Dye-Sensitized Solar Cells. *J. Alloys Compd.* **2015**, *622*, 1−7.

(25) Hod, I.; Shalom, M.; Tachan, Z.; Rühle, S.; Zaban, A. $SrTiO_3$ Recombination-Inhibiting Barrier Layer for Type II Dye-Sensitized Solar Cells. *J. Phys. Chem. C* **2010**, *114*, 10015−10018.

(26) Yang, S.; Kou, H.; Wang, J.; Xue, H.; Han, H. Tunability of the Band Energetics of Nanostructured $SrTiO_3$ Electrodes for Dye-Sensitized Solar Cells. *J. Phys. Chem. C* **2010**, *114*, 4245−4249.

(27) Wu, S.; Gao, X.; Qin, M.; Liu, J.-M.; Hu, S. $SrTiO_3$ Modified TiO_2 Electrodes and Improved Dye-Sensitized TiO_2 Solar Cells. *Appl. Phys. Lett.* **2011**, *99*, 042106.

(28) Diamant, Y.; Chen, S. G.; Melamed, O.; Zaban, A. Core-Shell Nanoporous Electrode for Dye Sensitized Solar Cells: The Effect of the $SrTiO_3$ Shell on the Electronic Properties of the TiO_2 Core. *J. Phys. Chem. B* **2003**, *107*, 1977−1981.

(29) Aponsu, G. M. L. P.; Wijayarathna, T. R. C. K.; Perera, I. K.; Perera, V. P. S.; Siriwardhana, C. P. K. The Enhancement of Photovoltaic Parameters in Dye-Sensitized Solar Cells of Nanocrystalline SnO_2 by Incorporating with Large $SrTiO_3$ Particles. *Spectrochim. Acta, Part A* **2013**, *109*, 37−41.

(30) Jayabal, P.; Sasirekha, V.; Mayandi, J.; Jeganathan, K.; Ramakrishnan, V. A Facile Hydrothermal Synthesis of $SrTiO_3$ for Dye Sensitized Solar Cell Application. *J. Alloys Compd.* **2014**, *586*, 456−461.

(31) Lenzmann, F.; Krueger, J.; Burnside, S.; Brooks, K.; Grätzel, M.; Gal, D.; Rühle, S.; Cahen, D. Surface Photovoltage Spectroscopy Of Dye-Sensitized Solar Cells with TiO_2, Nb_2O_5 and $SrTiO_3$ Nanocrystalline Photoanodes: Indication for Electron Injection from Higher Excited Dye States. *J. Phys. Chem. B* **2001**, *105*, 6347−6352.

(32) El Zayat, M.; Saed, A.; El-Dessouki, M. Photoelectrochemical Properties of Dye Sensitized Zr-Doped $SrTiO_3$ Electrodes. *Int. J. Hydrogen Energy* **1998**, *23*, 259−266.

(33) Sonntag, L. P.; Spitler, M. T. Examination of the Energetic Threshold for Dye-Sensitized Photocurrent at SrTiO$_3$ Electrodes. *J. Phys. Chem.* **1985**, *89*, 1453−1457.

(34) Tambo, T.; Maeda, K.; Shimizu, A.; Tatsuyama, C. Improvement of Electrical Properties of Epitaxial SrTiO$_3$ Films on Si(001)-2 × 1 by *In Situ* Annealing. *J. Appl. Phys.* **1999**, *86*, 3213−3217.

(35) Bao, D.; Yao, X.; Wakiya, N.; Shinozaki, K.; Mizutani, N. Band-Gap Energies of Sol-Gel-Derived SrTiO$_3$ Thin Films. *Appl. Phys. Lett.* **2001**, *79*, 3767−3769.

(36) Bhuiyan, M. N. K.; Kimura, H.; Tambo, T.; Tatsuyama, C. Growth of SrTiO$_3$ Films on Si(001)−Sr(2 × 1) Surfaces. *Appl. Surf. Sci.* **2005**, *249*, 419−424.

(37) Jalan, B.; Engel-Herbert, R.; Mates, T. E.; Stemmer, S. Effects of Hydrogen Anneals on Oxygen Deficient SrTiO$_{3−x}$ Single Crystals. *Appl. Phys. Lett.* **2008**, *93*, 052907.

(38) Park, T. J.; Kim, J. H.; Jang, J. H.; Lee, J.; Lee, S. W.; Lee, S. Y.; Jung, H. S.; Hwang, C. S. Effects of Annealing Environment on Interfacial Reactions and Electrical Properties of Ultrathin SrTiO$_3$ on Si. *J. Electrochem. Soc.* **2009**, *156*, G129−G133.

(39) Li, G.; Bai, Y.; Wu, S.; Zhang, W. Variation in Photocatalytic Activity of SrTiO$_3$(100) Single-Crystal Thin Films with Different Substrates and Annealing Atmosphere. *Sci. Adv. Mater.* **2013**, *5*, 764−768.

(40) Pal, P.; Kumar, P.; V, A.; Dogra, A.; Joshi, A. G. Chemical Potential Shift and Gap-State Formation in SrTiO$_{3−δ}$ Revealed by Photoemission Spectroscopy. *J. Appl. Phys.* **2014**, *116*, 053704.

(41) Sauvage, F.; Di Fonzo, F.; Li Bassi, A.; Casari, C. S.; Russo, V.; Divitini, G.; Ducati, C.; Bottani, C. E.; Comte, P.; Graetzel, M. Hierarchical TiO$_2$ Photoanode for Dye-Sensitized Solar Cells. *Nano Lett.* **2010**, *10*, 2562−2567.

(42) Noh, J. H.; Park, J. H.; Han, H. S.; Kim, D. H.; Han, B. S.; Lee, S.; Kim, J. Y.; Jung, H. S.; Hong, K. S. Aligned Photoelectrodes with Large Surface Area Prepared by Pulsed Laser Deposition. *J. Phys. Chem. C* **2012**, *116*, 8102−8110.

(43) Ghosh, R.; Brennaman, M. K.; Uher, T.; Ok, M.; Samulski, E. T.; McNeil, L. E.; Meyer, T. J.; Lopez, R. Nanoforest Nb$_2$O$_5$ Photoanodes for Dye-Sensitized Solar Cells by Pulsed Laser Deposition. *ACS Appl. Mater. Interfaces* **2011**, *3*, 3929−3935.

(44) Ghosh, R.; Brennaman, M. K.; Concepcion, J. J.; Hanson, K.; Kumbhar, A. S.; Meyer, T. J.; Lopez, R. Efficient High Surface Area Vertically Aligned Metal Oxide Nanostructures for Dye-Sensitized Photoanodes by Pulsed Laser Deposition. *Proc. SPIE* **2011**, *8109*, 81090U.

(45) Ghosh, R.; Hara, Y.; Alibabaei, L.; Hanson, K.; Rangan, S.; Bartynski, R.; Meyer, T. J.; Lopez, R. Increasing Photocurrents in Dye Sensitized Solar Cells with Tantalum-Doped Titanium Oxide Photoanodes Obtained by Laser Ablation. *ACS Appl. Mater. Interfaces* **2012**, *4*, 4566−4570.

(46) Hara, Y.; Garvey, T.; Alibabaei, L.; Ghosh, R.; Lopez, R. Controlled Seeding of Laser Deposited Ta:TiO$_2$ Nanobrushes and Their Performance as Photoanode for Dye Sensitized Solar Cells. *ACS Appl. Mater. Interfaces* **2013**, *5*, 13140−13145.

(47) Passoni, L.; Ghods, F.; Docampo, P.; Abrusci, A.; Martí-Rujas, J.; Ghidelli, M.; Divitini, G.; Ducati, C.; Binda, M.; Guarnera, S.; Li Bassi, A.; Casari, C. S.; Snaith, H. J.; Petrozza, A.; Di Fonzo, F. Hyperbranched Quasi-1D Nanostructures for Solid-State Dye-Sensitized Solar Cells. *ACS Nano* **2013**, *7*, 10023−10031.

(48) Kim, D. H.; Lee, S.; Park, J. H.; Noh, J. H.; Park, I. J.; Seong, W. M.; Hong, K. S. Transmittance Optimized Nb-doped TiO$_2$/Sn-doped In$_2$O$_3$ Multilayered Photoelectrodes for Dye-Sensitized Solar Cells. *Sol. Energy Mater. Sol. Cells* **2012**, *96*, 276−280.

(49) Kim, H.; Kushto, G. P.; Arnold, C. B.; Kafafi, Z. H.; Piqué, A. Laser Processing of Nanocrystalline TiO$_2$ Films for Dye-Sensitized Solar Cells. *Appl. Phys. Lett.* **2004**, *85*, 464−466.

(50) Lee, S.; Noh, J. H.; Han, H. S.; Yim, D. K.; Kim, D. H.; Lee, J.; Kim, J. Y.; Jung, H. S.; Hong, K. S. Nb-Doped TiO$_2$: A New Compact Layer Material for TiO$_2$ Dye-Sensitized Solar Cells. *J. Phys. Chem. C* **2009**, *113*, 6878−6882.

(51) Noh, J. H.; Lee, S.; Kim, J. Y.; Lee, J.-K.; Han, H. S.; Cho, C. M.; Cho, I. S.; Jung, H. S.; Hong, K. S. Functional Multilayered Transparent Conducting Oxide Thin Films for Photovoltaic Devices. *J. Phys. Chem. C* **2009**, *113*, 1083−1087.

(52) Ok, M.-R.; Ghosh, R.; Brennaman, M. K.; Lopez, R.; Meyer, T. J.; Samulski, E. T. Surface Patterning of Mesoporous Niobium Oxide Films for Solar Energy Conversion. *ACS Appl. Mater. Interfaces* **2013**, *5*, 3469−3474.

(53) Morisue, M.; Haruta, N.; Kalita, D.; Kobuke, Y. Efficient Charge Injection from the S2 Photoexcited State of Special-Pair Mimic Porphyrin Assemblies Anchored on a Titanium-modified ITO Anode. *Chem.—Eur. J.* **2006**, *12*, 8123−8135.

(54) Muthukumaran, K.; Loewe, R. S.; Ambroise, A.; Tamaru, S. I.; Li, Q.; Mathur, G.; Bocian, D. F.; Misra, V.; Lindsey, J. S. Porphyrins Bearing Arylphosphonic Acid Tethers for Attachment to Oxide Surfaces. *J. Org. Chem.* **2004**, *69*, 1444−1452.

(55) Watson, D. F.; Marton, A.; Stux, A. M.; Meyer, G. J. Influence of Surface Protonation on the Sensitization Efficiency of Porphyrin-Derivatized TiO$_2$. *J. Phys. Chem. B* **2004**, *108*, 11680−11688.

(56) Lu, H.-P.; Tsai, C.-Y.; Yen, W.-N.; Hsieh, C.-P.; Lee, C.-W.; Yeh, C.-Y.; Diau, E. W.-G. Control of Dye Aggregation and Electron Injection for Highly Efficient Porphyrin Sensitizers Adsorbed on Semiconductor Films with Varying Ratios of Coadsorbate. *J. Phys. Chem. C* **2009**, *113*, 20990−20997.

(57) Chen, Z.; Dinh, H. N.; Miller, E. *Photoelectrochemical Water Splitting*; Springer: New York, 2013.

(58) Swierk, J. R.; Mallouk, T. E. Design and Development of Photoanodes for Water-Splitting Dye-Sensitized Photoelectrochemical Cells. *Chem. Soc. Rev.* **2013**, *42*, 2357−2387.

(59) Song, W.; Brennaman, M. K.; Concepcion, J. J.; Jurss, J. W.; Hoertz, P. G.; Luo, H.; Chen, C.; Hanson, K.; Meyer, T. J. Interfacial Electron Transfer Dynamics For [Ru(bpy)$_2$((4,4′-PO$_3$H$_2$)$_2$bpy)]$^{2+}$ Sensitized TiO$_2$ in a Dye-Sensitized Photoelectrosynthesis Cell: Factors Influencing Efficiency and Dynamics. *J. Phys. Chem. C* **2011**, *115*, 7081−7091.

(60) Nayak, A.; Knauf, R. R.; Hanson, K.; Alibabaei, L.; Concepcion, J. J.; Ashford, D. L.; Dempsey, J. L.; Meyer, T. J. Synthesis and Photophysical Characterization of Porphyrin and Porphyrin−Ru(II) Polypyridyl Chromophore−Catalyst Assemblies on Mesoporous Metal Oxides. *Chem. Sci.* **2014**, *5*, 3115−3119.

(61) Jiang, S. W.; Zhang, Q. Y.; Li, Y. R.; Zhang, Y.; Sun, X. F.; Jiang, B. Structural Characteristics of SrTiO$_3$ Thin Films Processed by Rapid Thermal Annealing. *J. Cryst. Growth* **2005**, *274*, 500−505.

(62) Tse, Y. Y.; Koutsonas, Y.; Jackson, T. J.; Passerieux, G.; Jones, I. P. Microstructure of Homoepitaxial Strontium Titanate Films Grown by Pulsed Laser Deposition. *Thin Solid Films* **2006**, *515*, 1788−1795.

(63) Radecka, M.; Sobas, P.; Wierzbicka, M.; Rekas, M. Photo-electrochemical Properties of Undoped and Ti-Doped WO$_3$. *Phys. B* **2005**, *364*, 85−92.

(64) Morrison, S. R. *Electrochemistry of Semiconductor and Oxidized Metal Electrodes*; Plenum Press: New York, 1980.

(65) Yang, S.; Kou, H.; Wang, H.; Cheng, K.; Wang, J. Preparation and Band Energetics of Transparent Nanostructured SrTiO$_3$ Film Electrodes. *J. Phys. Chem. C* **2010**, *114*, 815−819.

(66) Ardo, S.; Meyer, G. J. Photodriven Heterogeneous Charge Transfer with Transition-Metal Compounds Anchored to TiO$_2$ Semiconductor Surfaces. *Chem. Soc. Rev.* **2009**, *38*, 115−164.

(67) Walters, L. C.; Grace, R. E. Formation of Point Defects in Strontium Titanate. *J. Phys. Chem. Solids* **1967**, *28*, 239−244.

(68) Yamada, H.; Miller, G. R. Point Defects in Reduced Strontium Titanate. *J. Solid State Chem.* **1973**, *6*, 169−177.

(69) McGuire, S.; Keeble, D. J.; Mason, R. E.; Coleman, P. G.; Koutsonas, Y.; Jackson, T. J. Variable Energy Positron Beam Analysis of Vacancy Defects in Laser Ablated SrTiO$_3$ Thin Films on SrTiO$_3$. *J. Appl. Phys.* **2006**, *100*, 044109.

(70) Khodan, A. N.; Guyard, S.; Contour, J. P.; Crété, D. G.; Jacquet, E.; Bouzehouane, K. Pulsed Laser Deposition of Epitaxial SrTiO$_3$ Films: Growth, Structure and Functional Properties. *Thin Solid Films* **2007**, *515*, 6422−6432.

(71) Ishiwata, K.; Mochizuki, S. Structural and Optical Properties of As-deposited and Annealed SrTiO$_3$ Films Prepared by Laser Ablation. *Phys. Status Solidi C* **2006**, *3*, 3516−3519.

(72) Almeida, B. G.; Pietka, A.; Mendes, J. A. Thin Films Deposited by Laser Ablation over Si Substrates. *Integr. Ferroelectr.* **2004**, *63*, 149−154.

(73) Chen, F.; Schafranek, R.; Li, S.; Wu, W. B.; Klein, A. Energy Band Alignment between Pb(Zr,Ti)O$_3$ and High and Low Work Function Conducting Oxides—From Hole to Electron Injection. *J. Phys. D: Appl. Phys.* **2010**, *43*, 295301.

(74) Kim, H. S.; Im, S. H.; Park, N. Organolead Halide Perovskite: New Horizons in Solar Cell Research. *J. Phys. Chem. C* **2014**, *118*, 5615−5625.

(75) Song, D.; Cui, P.; Wang, T.; Wei, D.; Li, M.; Cao, F.; Yue, X.; Fu, P.; Li, Y.; He, Y.; Jiang, B.; Trevor, M. Managing Carrier Lifetime and Doping Property of Lead Halide Perovskite by Postannealing Processes for Highly Efficient Perovskite Solar Cells. *J. Phys. Chem. C* **2015**, *119*, 22812−22819.

(76) Tachibana, Y.; Haque, S. A.; Mercer, I. P.; Durrant, J. R.; Klug, D. R. Electron Injection and Recombination in Dye Sensitized Nanocrystalline Titanium Dioxide Films: A Comparison of Ruthenium Bipyridyl and Porphyrin Sensitizer Dyes. *J. Phys. Chem. B* **2000**, *104*, 1198−1205.

(77) Chang, C. W.; Luo, L.; Chou, C. K.; Lo, C. F.; Lin, C. Y.; Hung, C. S.; Lee, Y. P.; Diau, E. W. G. Femtosecond Transient Absorption of Zinc Porphyrins with Oligo(phenylethylnyl) Linkers in Solution and on TiO$_2$ Films. *J. Phys. Chem. C* **2009**, *113*, 11524−11531.

(78) Imahori, H.; Kang, S.; Hayashi, H.; Haruta, M.; Kurata, H.; Isoda, S.; Canton, S. E.; Infahsaeng, Y.; Kathiravan, A.; Pascher, T.; Chábera, P.; Yartsev, A. P.; Sundström, V. Photoinduced Charge Carrier Dynamics of Zn-porphyrin−TiO$_2$ Electrodes: The Key Role of Charge Recombination for Solar Cell Performance. *J. Phys. Chem. A* **2011**, *115*, 3679−3690.

(79) Tachibana, Y.; Rubtsov, I. V.; Montanari, I.; Yoshihara, K.; Klug, D. R.; Durrant, J. R. Transient Luminescence Studies of Electron Injection in Dye Sensitised Nanocrystalline TiO$_2$ Films. *J. Photochem. Photobiol., A* **2001**, *142*, 215−220.